# Computational Study of Photosynthetic Pigments: Toward Synthetic Photosynthesis Engineering

# Adhityo Wicaksono<sup>1,2\*</sup>, Muhammad Ja'far Prakoso<sup>3</sup>, Afif Maulana Yusuf Ridarto<sup>4</sup>, and Arli Aditya Parikesit<sup>5\*\*</sup>

<sup>1</sup>Scientific Department, Genomik Solidaritas Indonesia Lab (GSI Lab), Jl. Sultan Agung No. 29, Setiabudi, Jakarta 12980, Indonesia

### \* Corresponding author:

email: adhityo.wicaksono@gsilab.id\*; arli.parikesit@i3l.ac.id\*\*

Received: February 28, 2025 Accepted: May 22, 2025

DOI: 10.22146/ijc.105059

**Abstract:** Chlorophyll is a widely known photosynthetic pigment in plants, algae, and cyanobacteria, along with bacteriochlorophyll in some photosynthetic bacteria. The pigments consist of tetrapyrrole structures that carry a single magnesium atom at the center. They play important parts in the light-harvesting process in photosynthesis. This study aimed to characterize and compare the electronic profiles of chlorophyll and bacteriochlorophyll pigments by using in silico computational approaches, such as density functional theory (DFT), electronic transfer property analysis, and protein-pigment interaction studies via molecular docking. The results showed that chlorophylls a, b, and c have the highest energy gaps at the ground state DFT. For bacteriochlorophylls, bacteriochlorophylls g and b have the highest energy gaps. The time-dependent DFT and the follow-up calculations, including extinction coefficient, tunneling rate, and coherence time, indicated bacteriochlorophyll g as a highly promising and efficient pigment. Additionally, chlorophyll c and bacteriochlorophylls c and d showed the strongest binding affinities with the chlorophyll-binding protein of plant photosystem II. This study provides a comprehensive and replicable computational pipeline for pigment profiling, advancing future synthetic photosynthesis designs through combined quantum and synthetic biology insights.

**Keywords:** exciton; photosystem; photosynthesis; quantum tunneling; quantum biology

#### **■ INTRODUCTION**

Chlorophyll is known as the group of pigments in cyanobacteria, algae, and plants that take the most important role in photosynthesis. Similarly, there is a bacteriochlorophyll group in photosynthetic bacteria. The pigments that consist of the tetrapyrrole structure, a single reduced version of the porphyrin ring called chlorine, and a double reduced version in bacteriochlorin contain a magnesium atom bound to the N4 center [1]. In the general process of light harvesting mechanism,

chlorophyll absorbs light, then conducts energy transfer by resonance energy transfer to the specific pair of chlorophyll molecules in the photosystem reaction center, which can perform charge separation and generate free protons (H<sup>+</sup>) and electrons (e<sup>-</sup>) [2] that drive photosynthesis forward [3]. Mainly, chlorophylls a and b, along with bacteriochlorophylls a, b, c, and d, are biosynthesized from the amino acid glutamate, which is shared with the heme and siroheme biosynthesis pathway and is part of the porphyrin metabolism

<sup>&</sup>lt;sup>2</sup>Biosciences and Biotechnology Research Center, Institut Teknologi Bandung, Jl. Ganesha No. 10, Bandung 40132, Indonesia

<sup>&</sup>lt;sup>3</sup>Theoretical and Computational Condensed Matter Physics Group, Department of Physics, Faculty of Mathematics and Natural Sciences, Universitas Indonesia, Depok 16424, Indonesia

<sup>&</sup>lt;sup>4</sup>Department of Materials and Metallurgical Engineering, Faculty of Industrial Technology and System Engineering, Institut Teknologi Sepuluh Nopember, ITS Sukolilo Campus, Surabaya 60111, Indonesia

<sup>&</sup>lt;sup>5</sup>Department of Bioinformatics, School of Life Sciences, Indonesia International Institute for Life Sciences, Jl. Pulomas Barat No. Kav. 88, RT. 4/RW. 9, Kayu Putih, Pulo Gadung, Jakarta 13210, Indonesia

pathway (KEGG pathway ID: map00860). Chlorophylls c, e.g., chlorophylls c1, c2, and c3, are biosynthesized as a branch from the biosynthetic pathway of chlorophyll a, specifically from protochlorophyllide that leads to chlorophyll a [4]. Chlorophylls d and f are synthesized from chlorophyllide a, precursor of chlorophyll a [5]. Bacteriochlorophylls c, d, and e can be found in green sulfur and green filamentous bacteria as their most abundant pigments, while bacteriochlorophyll g is the primary pigment in heliobacteria [6]. Both chlorophylls d and f belong to cyanobacteria [7-8]. Other pigments, such as chlorophyll e, are rare in Vaucheria hamata and Tribonema bombycinum [9]. Meanwhile. bacteriochlorophyll f, found in green sulfur bacteria, is evolutionarily unfavorable because their energy transfer is less efficient, causing slow growth [10].

The chlorophyll pigments are stored within protein complexes that work as the integrated light-harvesting machinery of photosynthesis. Chlorophyll a is the main chlorophyll pigment widely available in photosynthetic organisms [11]. Chlorophyll b is an accessory pigment available in plants, and the ratio compared to chlorophyll a is higher for shade-adapted chloroplasts [12]. In plants, chlorophylls a and b are stored inside the photosystem, specifically by chlorophyll-binding proteins [13]. Chlorophylls c are the chlorophyll pigments that can harvest blue and green light, allowing them to penetrate deeper water than other wavelengths, and are available in Chromista - a kingdom of eukaryotic algae [4]. These differences in pigment efficiency characteristics infer that specific pigments might be good in certain conditions. Additionally, if the photosynthetic organisms can be engineered to produce certain pigments, photosynthesis efficiency could improve, e.g., if the environment has lower or higher light intensity levels.

Plant photosynthesis is a process that involves quantum mechanical interactions, mainly the energy transfers between light (photon) and the excited electron (exciton). Upon hitting a chlorophyll or bacteriochlorophyll pigment, a photon causes an electron to excite from its molecular orbital, and while exhibiting quantum coherence properties in a wave function, the exciton transfers to other chlorophyll molecules until it

reaches the reaction center chlorophyll Hypothetically, each chlorophyll and bacteriochlorophyll molecule possesses unique quantum characteristics, e.g., frontier molecular orbitals (FMO) gaps that explain the distinctive energy gaps from the highest occupied molecular orbital (HOMO) to the lowest unoccupied molecular orbital (LUMO) [14]. These values characterize the molecular orbital excitation profiles at the ground state and time-dependent excitation energies using density functional theory (DFT) calculations. By understanding the different chlorophyll and bacteriochlorophyll profiles, the substitution of the pigments for future synthetic biology applications would be possible for enhanced photosynthetic system development.

The previous study focuses exclusively on chlorophylls a and b, analyzing their excited states in diethyl ether, acetone, and ethanol using TD-DFT with CAM-B3LYP functionals [15]. Their work emphasizes solvent polarity effects and functional tuning for these two pigments. Other studies have also simulated excitation energy profiles of chlorophyll [16-17], in chlorophylls d and f [18], and bacteriochlorophyll a [19]. This *in silico* study aimed to perform theoretical analysis via computational-based simulations and calculations to characterize different types of chlorophyll and bacteriochlorophyll pigments. A comprehensive dataset encompassing excitation energies, oscillator strengths, extinction coefficients and tunnelling rates across diverse pigments were generated from this study. This extensive analysis offers novel insights into the photophysical properties of these pigments under aqueous conditions, contributing valuable information for the design of synthetic light-harvesting systems. Moreover, in this study and analysis protocol, we attempted to use the simplified versions of the existing equations to make the data replicable and easily evaluated by interdisciplinary communities globally.

# **■ EXPERIMENTAL SECTION**

### **Materials**

The chlorophyll and bacteriochlorophyll molecules (Fig. 1) were obtained in SMILES format from the MetaCyc database (http://vm-trypanocyc.toulouse.inra.fr)

Fig 1. The structures of chlorophylls and bacteriochlorophylls with their various side chains (R)

and the Human Metabolome Database (HMDB) (https://hmdb.ca) in three-dimensional PDB format. Specifically, chlorophyll f was acquired from PubChem (CID: 122706135), and bacteriochlorophylls c and d were acquired from Chemical Entities of Biological Interest (ChEBI), with IDs of 60197 and 81553, respectively. The SMILES codes for bacteriochlorophylls and chlorophyll f were converted into a three-dimensional PDB format using the NIH NCI Online SMILES Translator (https://cactus.nci.nih.gov/translate). A protein used for docking was the photosystem II complex from Arabidopsis thaliana (PDB ID: 5MDX), which served as the scaffold for interactions with chlorophyll molecules.

### Instrumentation

Chlorophylls and bacteriochlorophylls molecules were prepared using Avogadro v1.2.0 (Avogadro Chemistry) for structural verification and energy minimization. The pigment molecules were analyzed using DFT with GaussView v6.0 and Gaussian 09W (Gaussian, Inc., US) [20]. For docking, energy-minimized pigment molecules were imported into the PyRx v0.8 pipeline (The Scripps Research Institute, US), including OpenBabel [21], for further energy minimization and

ligand conversion. Following the multiple ligands docking protocol, the ligands were docked into the protein scaffold using Autodock Vina [22].

The binding affinities from the three simulations were then analyzed statistically using SPSS Statistics (IBM, US) with an analysis of variance (ANOVA), followed by a post-hoc Duncan multiple range test to identify significant differences between pigments. The highest-scoring conformations, with the strongest binding affinities, were visualized using PyMOL v2.5.1 (Schrödinger, Inc., US) [23]. Lastly, all results were using the online **PCA** Calculator (https://www.statskingdom.com/pca-calculator.html) (Statistics Kingdom) to compare the data based on the correlations.

### **Procedure**

### **DFT** calculations

After energy minimization with Avogadro, the molecules were inputted into DFT calculations. In Avogadro, the Universal Force Field (UFF) was employed for the energy minimization, with the steepest descent algorithm applied in 4 steps per update. Frequency calculations were attempted to confirm the

absence of imaginary vibrational modes for selecting pigment structures. However, the jobs were not completed on the available local hardware due to the computational demands of vibrational analysis on large chromophores.

The DFT analysis was separated into three processes: (i) Ground state for initial identification of the FMO, [24] TD-DFT via time-dependent self-consistent field (TD-SCF) calculations for excited-state properties prediction, assuming default singlet spin states, under gas/non-solvent state, and (iii) another similar TD-DFT via TD-SCF (singlet spin states) with solvent effect. Becke's three-parameter exchange functional combined with the Lee-Yang-Parr correlation functional (B3LYP) [25-26] was employed, along with the basis set of 6-31G(d,p) for ground-state calculations, and Coulombattenuated method B3LYP (CAM-B3LYP) functional for TD-DFT as it facilitates long-range exchange interactions [27]. Additionally, a solvent model based on density (SMD) [28] for water solvent was applied to the TD-DFT second calculation solvent effect. From ground state calculations, the energy gaps between FMOs, namely HOMO and LUMO were recorded. From TD-DFT calculations, the key molecular properties, i.e., FMO, excitation energies, wavelength, oscillator strength and details about orbital transitions and energy gaps were obtained. For the TD-DFT with solvent effect, the same results observation was applied.

### **Post-DFT calculations**

Following the ground state and TD-DFT simulations, the obtained energy gaps of FMO (ground state DFT) and oscillator strength, frequency, and energy gaps (TD-DFT) were used as prerequisites for further calculations. This included the extinction coefficient (based on the oscillator strength) and tunneling rate.

$$\varepsilon = \frac{\varepsilon_{\text{coef}} \cdot f}{\lambda} \tag{1}$$

$$\varepsilon_{\text{coef}} = \frac{4\pi^2 N_A C^2}{\left(m_e c^2 \ln(10)\right)} \approx 4.32 \times 10^6 \,\text{M}^{-1} \text{cm}^{-1}$$
(2)

The molar extinction coefficient of the pigment ( $\epsilon$ ) (Eq. (1)) is calculated by incorporating the oscillator strength (f) and exciton wavelength ( $\lambda$ ) of the first excited state of the pigment resulting from the TD-DFT results, as

adapted from a previous study [29]. The universal extinction coefficient ( $\epsilon_{coef}$ ) (Eq. (2)) was obtained by measuring the various constants, e.g., Avogadro number ( $N_A$ ), elementary charge (C), electron mass ( $m_e$ ), and the speed of light (c).

To simulate the interaction profiling between the two same pigments (e.g., between two chlorophyll a), the tunneling rate (k<sub>ET</sub>) is calculated (Eq. (3)) based on Marcus' theory. The distance (d) was determined by using measurement features in PyMOL v3.0.3 (Schrödinger, Inc.) on A. thaliana photosystem II complex's (PDB ID: 5MDX) chlorophyll a, and the light harvesting complex's (PDB ID: 3BSD) bacteriochlorophyll a relative distance from each other (0.35 to 0.5 nm), a distance of 0.4 nm was selected as the rounded average distance. The exciton mass (me) or electron mass was used for the calculation. The preexponential factor (A) set at 1013 s-1 as the typical vibrational frequencies range was used. The pigment molecular barrier energy (Ebarrier) was determined by dividing the energy gap into two (Eq. (4)), assuming the energy barrier that separates two molecules is ideal.

$$k_{ET} = A \cdot e^{-\frac{2d\sqrt{2m_e(E_{barrier})}}{\hbar}}$$
(3)

$$E_{\text{barrier}} = \frac{E_g}{2} \tag{4}$$

Lastly, the coherent time  $(\tau_c)$  was calculated by using the energy-time uncertainty principle, with the energy uncertainty being the energy barrier of the system ( $\Delta E$ ) (Eq. (5)).

$$\tau_{\rm c} = \frac{\hbar}{\Delta E} \tag{5}$$

## Molecular docking result analysis

Following the molecular docking, binding affinities, root-mean-square deviation (RMSD) values, hydrogen bonds and hydrophobic interactions (van der Waals forces) were recorded for each docking run. Blind docking tests were conducted to assess the binding sites of each pigment (e.g., chlorophyll a) within the active site of a chlorophyll-binding photosystem II protein receptor. The docking simulations were repeated three times to ensure statistical accuracy. Key hydrogen bonds and hydrophobic interactions for each pigment were

compared. The primary objective for docking was not to validate the *in vivo* binding under physiological conditions but to assess and compare theoretical binding affinities as a predictive screening tool. This analysis supports future synthetic biology applications, particularly in designing or modifying light-harvesting protein–pigment complexes where alternative pigments may be incorporated. Such comparative data can guide pigment substitution strategies by identifying molecules with favorable protein-binding propensities prior to experimental implementation.

### Additional statistics

Once the values for the ground state DFT FMO energy gap, the values from TD-DFT, such as extinction coefficient, tunneling rate, coherent time, and docking binding affinity, were obtained, a two-dimensional principal component analysis (PCA) of correlation (eigenvalue decomposition) with standardized values (to the mean and standard deviation) was generated and visualized.

### RESULTS AND DISCUSSION

# Chlorophyll Structural Significance and FMO Profiles

Chlorophyll is essential for photosynthesis, with various types (a, b, and c) playing distinct roles in light absorption and energy conversion. Chlorophyll a, the primary pigment in most photosynthetic organisms, absorbs light most effectively in the blue-violet (around 430 nm) and red (around 662 nm at Q<sub>v</sub> band) parts of the spectrum. This absorption enables chlorophyll a to drive photosynthesis by capturing light energy and converting it into chemical energy through electron transport. In contrast, chlorophyll b acts as an accessory pigment, extending the range of light usable for photosynthesis by absorbing additional wavelengths in the blue and redorange regions (around 453 and 642 nm) [30]. Chlorophyll c, found primarily in algae, lacks the hydrophobic phytol chain present in chlorophyll a and b, making it more water-soluble and thus better suited for aquatic environments in which algae thrive. The structural differences in chlorophyll c allow it to absorb wavelengths that are less accessible to chlorophyll a, particularly in environments where light is filtered through water [31-33]. A previous study revealed that chlorophyll f has an absorption spectrum peaking at 740 nm [34]. Similarly, bacteriochlorophylls c, d, and e absorb in the range of 650 to 800 nm [35].

Further research into magnesium porphyrins is needed, as the core structures of chlorophyll molecules highlight the central role of the magnesium ion in stabilizing the porphyrin ring. This stabilization is crucial for the efficient absorption of light and the subsequent transfer of electrons during photosynthesis, as seen in chlorophyll a and its accessory pigments [36]. This variation in structure and function allows plants and algae to optimize light absorption across a range of environmental conditions, particularly in low-light or water-filtered environments. Previous studies [36-37] have provided critical insights into how these chlorophyll molecules adapt to different ecological niches, enhancing their efficiency in capturing and converting light energy for photosynthesis.

The chlorophylls and bacteriochlorophylls studied in this research show distinct electronic characteristics based on their molecular structures, which were visualized using DFT calculations at the ground state. These pigments contain tetrapyrrole rings (either chlorin, phytochlorin, porphyrin, or bacteriochlorin), with a central magnesium ion playing a crucial role in stabilizing the ring structure and facilitating light absorption during photosynthesis [1].

The chemistry behind these structures lies in their electronic properties. The tetrapyrrole rings in chlorophylls a, b, d, and f (and bacteriochlorophylls a, b, and g) serve as the primary sites for electron excitation. The delocalized  $\pi$ -electrons within these rings are responsible for absorbing light and enabling the excitation of electrons from the HOMO to the LUMO, which is essential for the photochemistry of photosynthesis [38].

The FMO analysis (Fig. 2 and 3) reveals that the electron density is concentrated around the tetrapyrrole rings of both chlorophylls and bacteriochlorophylls, particularly in their HOMO and LUMO regions. This distribution of electron density affects the pigments'

ability to absorb light at different wavelengths. The summarized energy gaps between the HOMO and LUMO

for each pigment (Table 1) indicate the amount of energy required for electronic transitions.

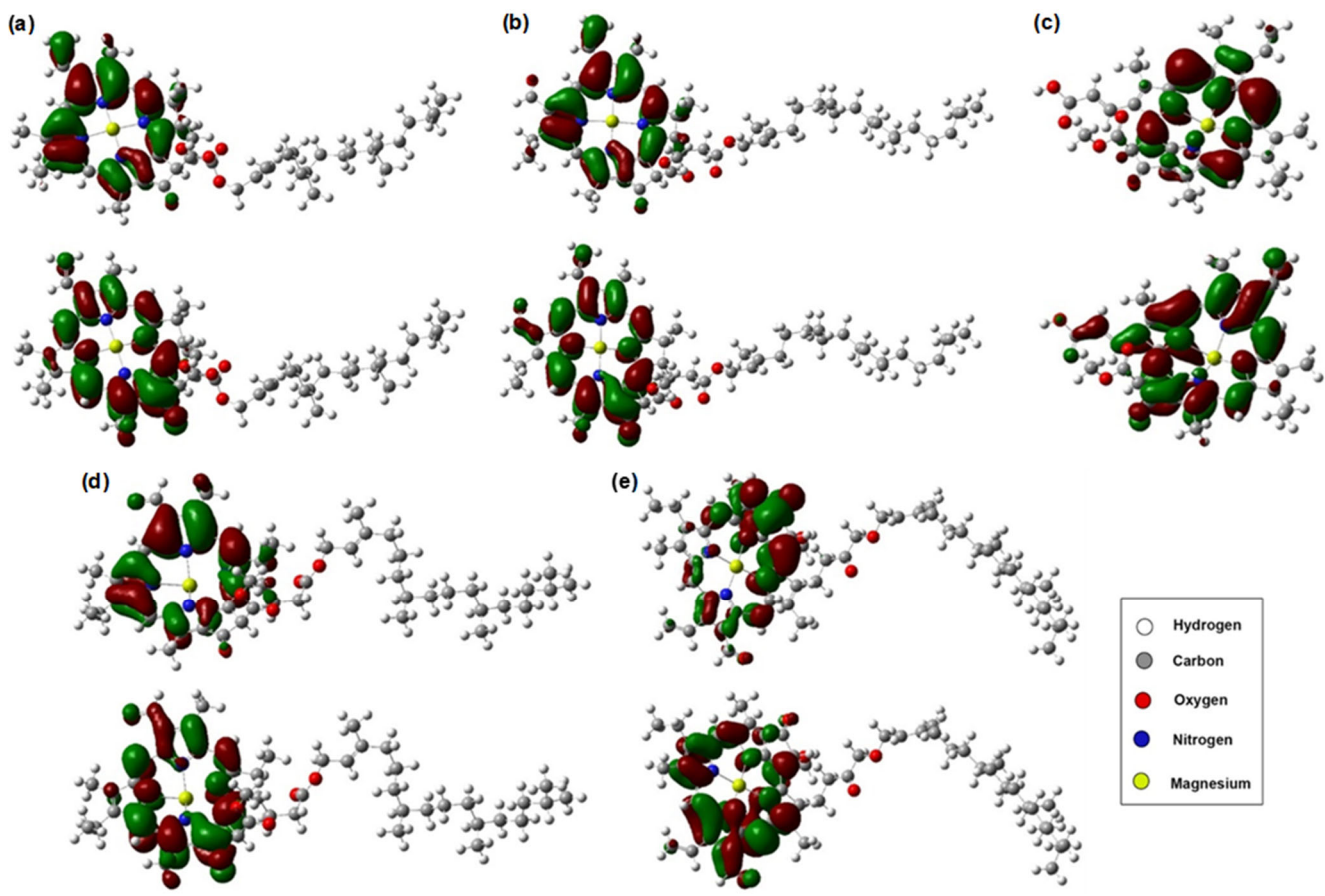
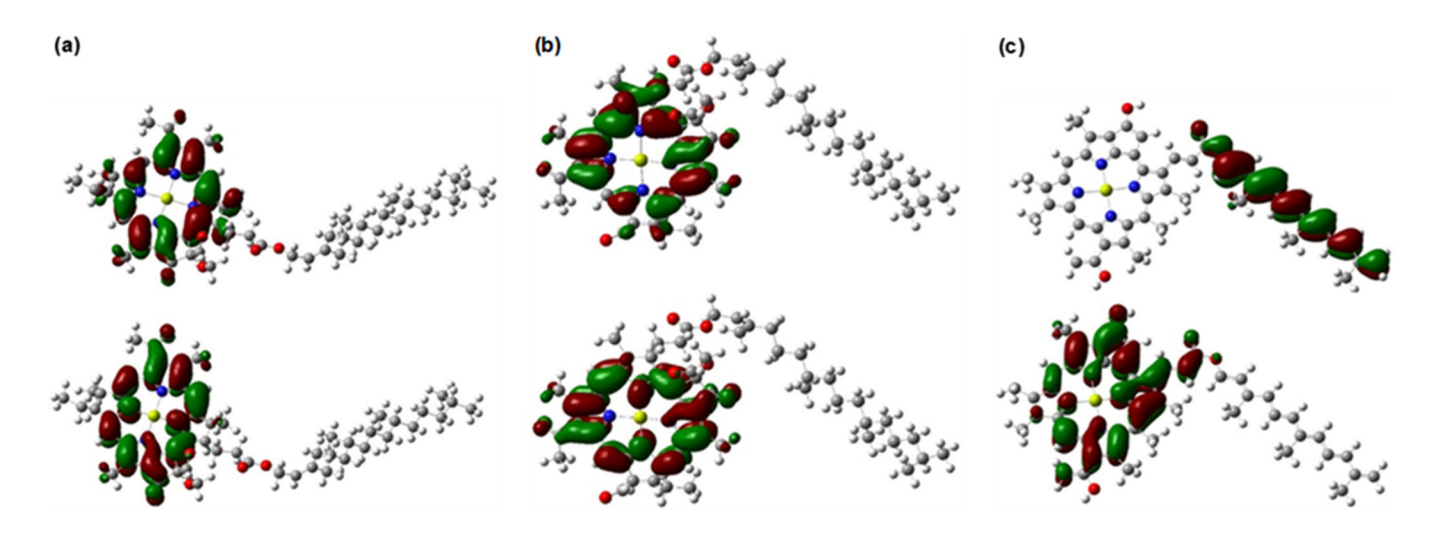
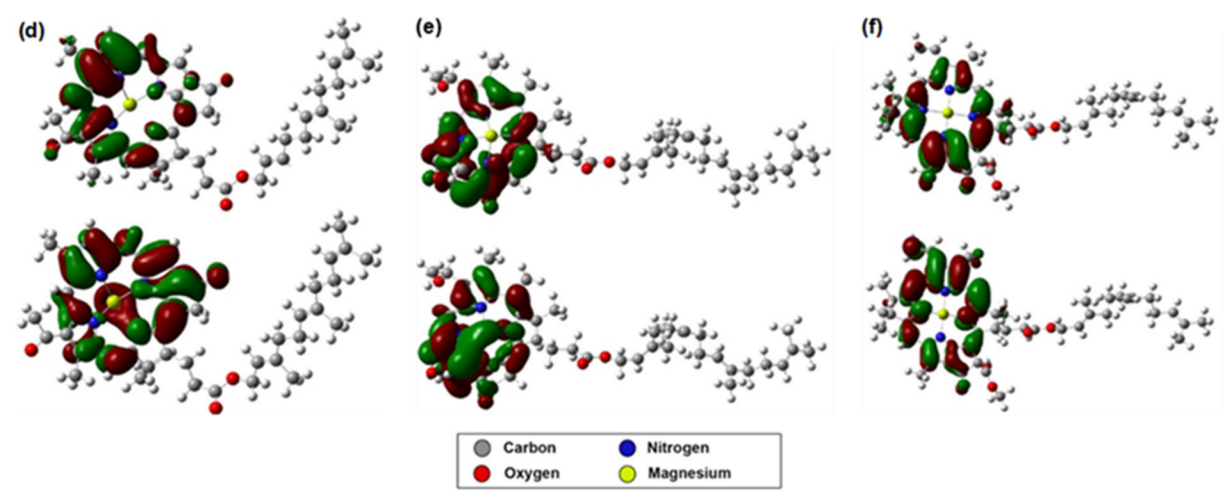


Fig 2. Chlorophyll frontier molecular orbital profiles (on each, HOMO on top and LUMO on bottom), showing the electron density dispersed surrounding the tetrapyrrole ring structures of the pigments (a–e): chlorophylls a, b, c, d, and f





**Fig 3.** Bacteriochlorophyll frontier molecular orbital profiles (on each, HOMO on top and LUMO on bottom), showing the electron density also dispersed surrounding the tetrapyrrole ring structures of the pigments as previously observed in the chlorophylls whereas (a–f): bacteriochlorophylls a, b, c, d, e, and g

**Table 1.** Frontier molecular orbital and the energy gap profiles at the ground state

Pigments	FMO	Energy (eV)	FMO E <sub>gap</sub> (eV)
Chl a	HOMO	-4.921	2.247
	LUMO	-2.674	
Chl b	HOMO	-5.069	2.265
	LUMO	-2.804	
Chl c	HOMO	-5.083	2.661
	LUMO	-2.423	
Chl d	HOMO	-4.989	2.360
	LUMO	-2.630	
Chl f	HOMO	-3.976	0.549
	LUMO	-3.427	
BChl a	HOMO	-4.534	1.721
	LUMO	-2.813	
BChl b	HOMO	-4.679	1.702
	LUMO	-2.977	
BChl c	HOMO	-4.250	0.830
	LUMO	-3.420	
BChl d	HOMO	-5.264	0.652
	LUMO	-4.612	
BChl e	HOMO	-4.333	1.057
	LUMO	-3.276	
BChl g	HOMO	-4.509	2.109
	LUMO	-2.400	

Note: Chl - chlorophyll, BChl - bacteriochlorophyll

The HOMO-LUMO gaps of chlorophyll pigments reveal essential insights into their absorption properties. Chlorophyll a, with a HOMO-LUMO gap of 2.247 eV,

absorbs light around 605 nm, placing it in the red region of the spectrum, making it highly effective for capturing red light during photosynthesis. Chlorophyll b, with a slightly larger gap of 2.265 eV, absorbs light around 606 nm and serves as an accessory pigment, extending the range of light plants can utilize. Chlorophyll c, commonly found in algae, has a HOMO-LUMO gap of 2.661 eV, enabling it to absorb shorter wavelengths around 550 nm, allowing algae to thrive in deeper water environments where blue and green light is more prevalent. Chlorophylls d and f, primarily found in cyanobacteria, exhibit unique absorption characteristics. Chlorophyll d absorbs around 596 nm, while chlorophyll f, with the smallest energy gap of 0.549 eV, absorbs far-infrared light. This allows it to function efficiently in low-light environments. These structural variations contribute to the diverse roles in photosynthesis, enabling organisms to adapt to various light conditions.

### **Exciton Energy Profiles**

The exciton energy profiles for each chlorophyll pigment were calculated using TD-DFT using CAM-B3LYP/6-31G(d,p) under non-solvent (gas phase) and SMD ( $\rm H_2O$ ) solvent condition (Table 2). The result revealed important details about their absorption properties. Exciton energies represent the energy required for an electron to be excited from the ground state to a

Table 2. Exciton energy profiles of each pigment under no solvent and with solvent (H<sub>2</sub>O)

-			No solvent	<u> </u>	Solvent effect: SMD-H <sub>2</sub> O		Differences (H <sub>2</sub> O vs gas)			
Pigment	Excited	Energy	Wavelength	Oscillator	Energy	Wavelength	Oscillator	ΔEnergy	Wavelength	Oscillator
· ·	state	(eV)	(nm)	strength (f)	(eV)	(nm)	strength (f)	(eV)	(nm)	strength (f)
Chl a	1	2.1816	568.32	0.2913	2.1450	578.02	0.3811	-0.0366	9.70	0.0898
	2	2.4526	505.52	0.0906	2.3918	518.38	0.2024	-0.0608	12.86	0.1118
	3	3.3222	373.20	0.0610	3.3328	372.01	0.6463	0.0106	-1.19	0.5853
Chl b	1	2.1376	580.03	0.2403	2.0797	596.15	0.3325	-0.0579	16.12	0.0922
	2	2.4438	507.35	0.0595	2.3868	519.45	0.1684	-0.0570	12.10	0.1089
	3	3.1836	389.45	0.7274	3.0763	403.03	0.7435	-0.1073	13.58	0.0161
Chl c	1	2.3979	517.06	0.0240	2.3568	526.07	0.0960	-0.0411	9.01	0.0720
	2	2.5487	486.46	0.0343	2.5829	480.02	0.0632	0.0342	-6.44	0.0289
	3	2.8032	442.29	0.0231	3.1715	390.93	0.8896	0.3683	-51.36	0.8665
Chl d	1	2.2946	540.33	0.1687	2.2272	556.67	0.2321	-0.0674	16.34	0.0634
	2	2.4336	509.47	0.1420	2.3762	521.77	0.3181	-0.0574	12.30	0.1761
	3	2.5115	493.67	0.0245	3.3354	371.73	0.4111	0.8239	-121.94	0.3866
Chl f	1	0.3367	3682.40	0.0016	1.1472	1080.71	0.0104	0.8105	-2601.69	0.0088
	2	1.8093	685.27	0.1252	2.1774	569.43	0.1804	0.3681	-115.84	0.0552
	3	2.0234	612.76	0.1700	2.4425	507.61	0.3569	0.4191	-105.15	0.1869
BChl a	1	1.5665	791.49	0.3580	1.4175	874.65	0.4872	-0.1490	83.16	0.1292
	2	2.3218	534.00	0.0834	2.2295	556.10	0.1572	-0.0923	22.10	0.0738
	3	3.3278	372.57	0.0015	3.2679	379.40	0.6510	-0.0599	6.83	0.6495
BChl b	1	1.5373	806.51	0.3543	1.4042	882.98	0.4793	-0.1331	76.47	0.1250
	2	2.3163	535.28	0.0933	2.2274	556.63	0.1683	-0.0889	21.35	0.0750
	3	3.2653	379.71	0.0051	3.2868	377.22	0.0483	0.0215	-2.49	0.0432
BChl c	1	1.7982	689.50	0.0509	1.7975	689.75	0.0855	-0.0007	0.25	0.0346
	2	2.1952	564.79	0.0104	2.2061	562.01	0.0248	0.0109	-2.78	0.0144
	3	2.8766	431.00	0.0233	2.8485	435.26	0.7914	-0.0281	4.26	0.7681
BChl d	1	0.2245	5521.90	0.0070	0.6548	1893.48	0.0269	0.4303	-3628.42	0.0199
	2	0.9363	1324.16	0.0065	1.7875	693.61	0.3791	0.8512	-630.55	0.3726
	3	1.5094	821.43	0.2236	2.0344	609.44	0.0368	0.5250	-211.99	-0.1868
BChl e	1	0.4743	2613.92	0.0089	0.6471	1915.89	0.0134	0.1728	-698.03	0.0045
	2	1.4476	856.47	0.0451	1.4530	853.31	0.0957	0.0054	-3.16	0.0506
	3	2.0197	613.87	0.0003	2.2552	549.77	0.0003	0.2355	-64.10	0.0000
BChl g	1	2.2129	560.27	0.2862	2.4484	506.39	0.3766	0.2355	-53.88	0.0904
	2	2.6153	474.07	0.1210	2.5934	478.07	0.2365	-0.0219	4.00	0.1155
	3	3.4308	361.39	0.0081	3.3494	370.17	0.0424	-0.0814	8.78	0.0343

Note: Chl - Chlorophyll, BChl - Bacteriochlorophyll

higher energy state and are a key factor in understanding the light-harvesting efficiency of photosynthetic pigments. Additionally, the changes on wavelengths due to solvent effect, whether redshifted (shifted to longer wavelength) or blue-shifted (shifted to shorter wavelength), could also reflect the pigment characteristics. The transitional details of electron excitation energies are available in Table S1 and S2.

For chlorophyll a, the first excited state exhibited a redshift from 568.32 to 578.02 nm ( $\Delta\lambda$  = +9.7 nm) with a significant increase in oscillator strength from 0.2913 to

0.3811 in solvent. This enhancement supports its robust light absorption in aqueous photosynthetic environments. Chlorophyll b followed a similar trend with a shift from 580.03 to 596.15 nm and an oscillator increase of +0.0922, reinforcing its complementary role in broadening the absorption range. Chlorophyll c, which is more prevalent in marine algae [4], showed a smaller redshift (+9.01 nm) in its first transition but exhibited a remarkable intensity increase in its third excited state (f rose from 0.0231 to 0.8896), suggesting solvent-enhanced charge transfer or  $\pi$ + $\pi$ \* character.

Chlorophylls d and f displayed even more dramatic solvent effects. Chlorophyll d's third state experienced a blue shift of -121.94 nm (from 493.67 to 371.73 nm), while chlorophyll f, previously showing extremely long-wavelength absorption in the gas phase (3682.4 nm), was blue-shifted in solvent to 1080.71 nm, bringing its transition into the near-infrared range. This unique absorption spectrum allows chlorophyll f to function efficiently in environments with very low light levels dominated by far-red photons [39].

Among the bacteriochlorophylls, bacteriochlorophylls a and b showed enhanced absorption strength and modest redshifts in their first transitions (+83.16 and +76.47 nm, respectively). Bacteriochlorophyll d, however, underwent a substantial blue shift of -3628.42 nm in its first excitation, correcting its gas-phase far-infrared prediction toward more biologically relevant wavelengths. Similarly, bacteriochlorophyll e showed solvent stabilization, with a wavelength shift of -698.03 nm and improved intensity ( $\Delta f = +0.0045$ ). Interestingly, bacteriochlorophyll g, the pigment associated with far-red adapted phototrophs, exhibited a blue shift in its first excitation (–53.88 nm) and increased oscillator strength (+0.0904), suggesting an environmentally responsive tuning of its absorption. These solvent-dependent shifts highlight how local dielectric environments may be crucial for tuning absorption profiles in natural systems [15]. Overall, the TD-DFT data confirms that solvent effects are quantitatively significant and may qualitatively reshape the absorption landscape of specialized chlorophylls and bacteriochlorophylls, especially those adapted to low-light or extreme environments.

### **Additional Calculations**

The extinction coefficient (molar extinction coefficient) was calculated to observe the strength of the pigment in absorbing light at the specific wavelength, which in this case is the exciton spectrum wavelength. The calculated extinction coefficients from the first excited state (Table 3) reveal that chlorophyll a, bacteriochlorophylls a and g exhibit the highest light

**Table 3.** Calculation results of the extinction coefficient from the first excited state of all the pigments in Table 2

Conditions	Diamont	TD-DFT FMO	Wavelength	Oscillator	Extinction coefficient
Conditions	Pigment	energy gap (eV)	(nm)	strength (f)	(L/mol·cm)
No Solvent	Chlorophyll a	3.997	568.32	0.2913	$2.214 \times 10^{10}$
	Chlorophyll b	4.015	580.03	0.2403	$1.790 \times 10^{10}$
	Chlorophyll c	4.590	517.06	0.0240	$2.005 \times 10^9$
	Chlorophyll d	4.206	540.33	0.1687	$1.349 \times 10^{10}$
	Chlorophyll f	2.161	3682.40	0.0016	$1.877 \times 10^{7}$
	Bacteriochlorophyll a	3.228	791.49	0.3580	$1.954 \times 10^{10}$
	Bacteriochlorophyll b	3.214	806.51	0.3543	$1.898 \times 10^{10}$
	Bacteriochlorophyll c	4.041	689.50	0.0509	$3.189 \times 10^9$
	Bacteriochlorophyll d	1.995	5521.90	0.0070	$5.476 \times 10^{7}$
	Bacteriochlorophyll e	2.962	2613.92	0.0089	$1.471 \times 10^{8}$
	Bacteriochlorophyll g	3.937	560.27	0.2862	$2.207 \times 10^{10}$
Solvent (SMD =	Chlorophyll a	4.026	578.02	0.3811	$2.848 \times 10^{10}$
H <sub>2</sub> O)	Chlorophyll b	4.020	596.15	0.3325	$2.409 \times 10^{10}$
	Chlorophyll c	4.492	526.07	0.0960	$7.883 \times 10^9$
	Chlorophyll d	4.213	556.67	0.2321	$1.801 \times 10^{10}$
	Chlorophyll f	2.943	1080.71	0.0104	$4.157 \times 10^{8}$
	Bacteriochlorophyll a	3.132	874.65	0.4872	$2.406 \times 10^{10}$
	Bacteriochlorophyll b	3.142	882.98	0.4793	$2.345 \times 10^{10}$
	Bacteriochlorophyll c	3.926	689.75	0.0855	$5.355 \times 10^9$
	Bacteriochlorophyll d	2.427	1893.48	0.0269	$6.137 \times 10^{8}$
	Bacteriochlorophyll e	3.107	1915.89	0.0134	$3.021 \times 10^{8}$
	Bacteriochlorophyll g	4.241	506.39	0.3766	$3.213 \times 10^{10}$

absorption capacity, consistent with their known roles as principal pigments in plant and bacterial photosystems. Notably, bacteriochlorophyll g, although less commonly discussed, showed an exceptionally high extinction coefficient in water  $(3.21 \times 10^{10} \text{ L/mol cm})$ , comparable to chlorophyll a, suggesting strong absorption even under far-red conditions. In contrast, pigments like chlorophylls c, f, and bacteriochlorophylls d-e demonstrated much lower extinction values, especially under gas-phase conditions. However, solvent effects (SMD H<sub>2</sub>O) enhanced the extinction coefficients of nearly all pigments, with chlorophyll c increasing more than 3-fold and bacteriochlorophyll g showing the most significant absolute gain. This trend reflects how solvent polarity and dielectric environment can intensify dipole-allowed transitions and highlights the ecological tuning of pigments: high extinction in key wavelengths is likely favored in pigments central to primary light harvesting. In contrast, others may serve in supportive or adaptive roles where spectral breadth or low-light specialization is prioritized.

The tunneling rates of the pigments also indicate the transfer rate between pigments, assuming a fixed inter-pigment gap of 0.4 nm (Table 4). At the same time, faster coherent time suggests rapid energy transfer but greater sensitivity to decoherence. In general, pigments with lower energy barriers exhibit faster tunneling rates and longer coherent lifetimes, suggesting more favorable quantum energy transfer characteristics. Among all, bacteriochlorophyll d shows the lowest energy barrier (0.997 eV in gas phase; 1.213 eV in solvent), resulting in the fastest tunneling (5.147  $\times$  10<sup>13</sup> to 6.093  $\times$  10<sup>13</sup> s<sup>-1</sup>) and longest coherence time  $(6.599 \times 10^{-16} \text{ to } 5.424 \times 10^{-16} \text{ s})$ . In contrast, chlorophyll c displays higher energy barriers (2.29 eV in gas; 2.25 eV in water), correlating with faster decoherence and lower tunneling rates, potentially due to its more delocalized excitation profile. Both chlorophyll a and bacteriochlorophyll a, the central pigments in oxygenic and anoxygenic photosynthesis, respectively, strike a balance, offering moderately low energy barriers and coherent times in the range of ~3- $4 \times 10^{-16}$  s, aligning with their observed high extinction

**Table 4.** Tunneling rates and coherent time of the pigments among themselves, assuming the gap between pigments is equal to 0.4 nm

Conditions	Pigment pair	Energy barrier (eV)	Tunnelling bate $(s^{-1}; in \times 10^{13})$	Coherent time (s; in $\times 10^{-16}$ )
No Solvent	Chlorophyllo	` '	10.166	
No solvent	Chlorophyll a - a	1.998		3.294
	Chlorophyll b - b	2.008	10.222	3.279
	Chlorophyll c - c	2.295	12.004	2.868
	Chlorophyll d - d	2.103	10.795	3.130
	Chlorophyll f - f	1.080	5.503	6.092
	Bacteriochlorophyll a - a	1.614	8.038	4.078
	Bacteriochlorophyll b - b	1.607	8.002	4.096
	Bacteriochlorophyll c - c	2.021	10.299	3.257
	Bacteriochlorophyll d - d	0.997	5.147	6.599
Solvent (SMD = $H_2O$ )	Bacteriochlorophyll e - e	1.481	7.362	4.445
	Bacteriochlorophyll g - g	1.969	9.992	3.344
	Chlorophyll a - a	2.013	10.253	3.270
	Chlorophyll b - b	2.010	10.237	3.274
	Chlorophyll c - c	2.246	11.690	2.930
	Chlorophyll d - d	2.106	10.815	3.125
	Chlorophyll f - f	1.472	7.317	4.472
	Bacteriochlorophyll a - a	1.566	7.791	4.203
	Bacteriochlorophyll b - b	1.571	7.815	4.190
	Bacteriochlorophyll c - c	1.963	9.959	3.353
	Bacteriochlorophyll d - d	1.213	6.093	5.424
	Bacteriochlorophyll e - e	1.553	7.727	4.237
	Bacteriochlorophyll g - g	2.120	10.901	3.104

coefficients (Table 3). This coupling of strong light absorption and efficient quantum tunneling underscores their evolutionary optimization for primary energy capture and transfer. Interestingly, while chlorophyll f and bacteriochlorophyll e have lower extinction coefficients, they maintain relatively prolonged coherence times (up to  $\sim 4.4-6.6\times 10^{-16}\,\mathrm{s}$ ), suggesting they may support specialized roles where long-lived but slower energy transfer is advantageous, such as in low-light or near-infrared environments. Together, these results reinforce the idea that efficient energy transfer is not solely determined by light absorption, but also by a pigment's quantum mechanical profile, highlighting the interplay between molecular structure, environment, and quantum dynamics.

The excitation profiles, extinction coefficients, and tunneling-coherence dynamics (Table 2-4) reveal how each pigment uniquely balances light absorption with quantum efficiency. Chlorophyll transfer bacteriochlorophyll a, and bacteriochlorophyll g stand out with strong light-harvesting capacity, solventenhanced oscillator strengths, and fast, coherent tunneling, ideal for bright, energy-rich environments. In chlorophyll contrast, pigments like bacteriochlorophyll d display weaker absorption but compensate with longer coherent lifetimes and lower tunneling barriers, pointing to roles in low-light or far-red conditions. So, for synthetic photosystems designed for environments, chlorophyll bright-light bacteriochlorophyll g offer optimal performance. In contrast, chlorophyll f and bacteriochlorophyll d are better suited for darker or filtered-light settings due to their quantum resilience and far-red adaptation.

# **Molecular Docking Results**

Molecular docking simulations were performed to assess the interactions between different chlorophylls and bacteriochlorophylls with the chlorophyll-binding protein scaffold of the Photosystem II complex in *A. thaliana* (PDB ID: 5MDX). The binding affinities, the number of hydrogen bonds, and hydrophobic/van der Waals interactions were analyzed (Fig. 4). The docking resulted in molecular binding affinities with the protein (Fig. 4(a)). The strength of these affinities appears to be

influenced by the number of contributing hydrogen bonds (Fig. 4(b)) and the hydrophobic or van der Waals interactions within the protein cavity (Fig. 4(c)). Chlorophyll c displayed the highest binding affinity (-10.27 kcal/mol). Still, it formed no hydrogen bonds and had the lowest number of hydrophobic interactions (8 interactions). Chlorophyll d had the second-highest binding affinity (-8.87 kcal/mol), forming 2 hydrogen bonds and 14 hydrophobic interactions. In contrast, chlorophyll f had a lower binding affinity (-7.83 kcal/mol), forming 1 hydrogen bond and 13 hydrophobic interactions. Among the bacteriochlorophylls, bacteriochlorophyll d had the highest binding affinity (-10.13 kcal/mol), forming 1 hydrogen bond and 14 hydrophobic interactions. Bacteriochlorophyll e, with a binding affinity of -9.13 kcal/mol, formed 4 hydrogen bonds and 12 hydrophobic interactions, the highest number of hydrogen bonds among all ligands. Bacteriochlorophyll demonstrated strong binding (-9.80 kcal/mol), forming 2 hydrogen bonds and 11 hydrophobic interactions. However, statistical analysis difference indicated no significant between bacteriochlorophylls c and d.

Chlorophylls a and b, which are commonly involved in photosynthesis, had moderate binding affinities (-8.40 and -8.47 kcal/mol, respectively, and their value differences are statistically not significant), both forming 1-2 hydrogen bonds and engaging in 13-14 hydrophobic interactions. These interactions suggest a stable and energetically favorable docking, especially for chlorophyll a, which primarily influences light absorption during photosynthesis. The results also showed that bacteriochlorophylls generally exhibit stronger binding affinities compared to chlorophylls.

## **Principal Component Analysis**

PCA analysis was conducted to evaluate the profile similarities of the pigments based on correlation through plots of the eigenvalues. PCA analysis visualization (Fig. 5(a)) revealed that the tunneling rate and energy gap (ground state DFT) eigenvalues overlap closely, followed by those of binding affinity and extinction coefficient and those of coherent time. The PCA results of ten keys

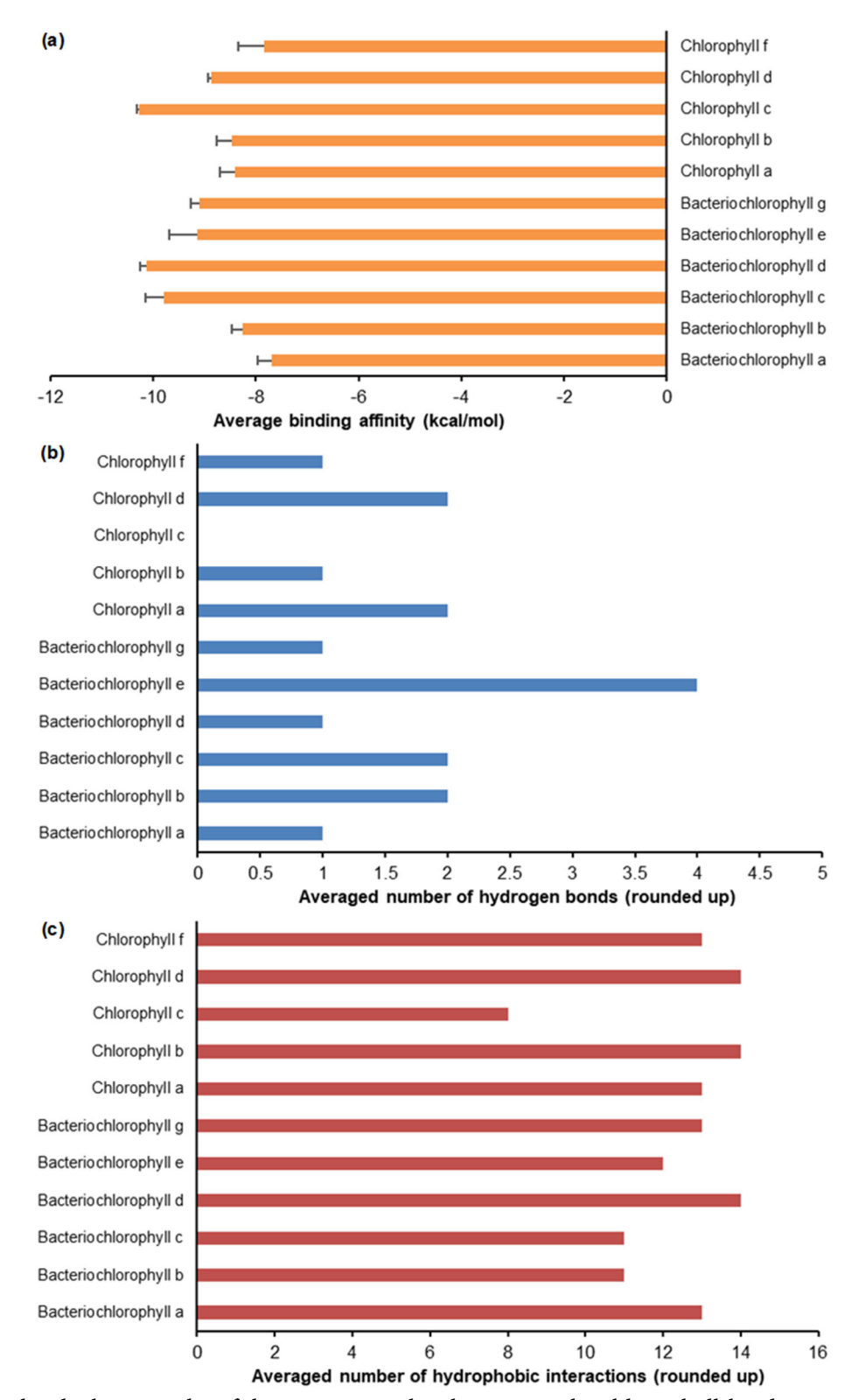


**Fig 4.** The molecular docking results of the pigment molecules against the chlorophyll-binding protein that served as the protein scaffold indicated the comparisons of (a) average binding energies, (b) rounded-up averaged values of hydrogen bonds, and (c) rounded-up averaged values of the hydrophobic interactions

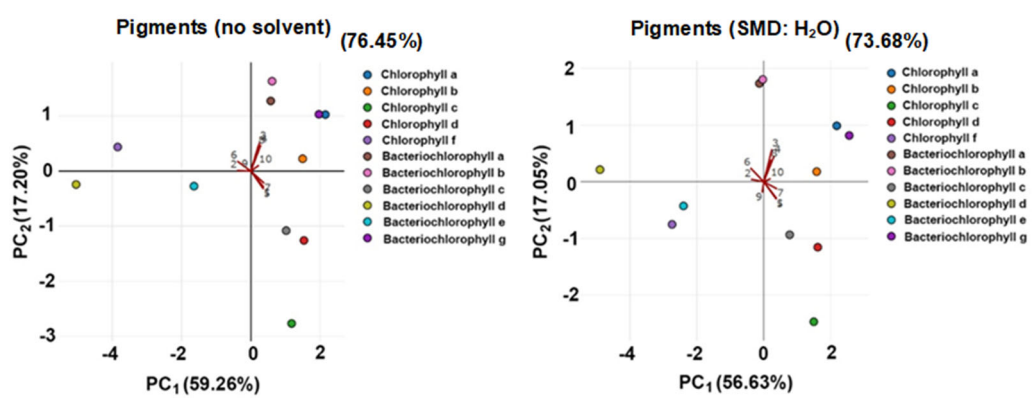


Fig 5. PCA of 10 observed characteristics of all pigments in (a) no-solvent phase and (b) simulated under SMD solvent effect with water. Notes: The calculation is based on the TD-DFT results at the 1st state, where excitation states between HOMO and LUMO are all present. Eigenvector letters: TD-DFT FMO energy gap (1), wavelength (2), oscillator strength (3), extinction coefficient (4), trans-pigment tunneling rate (5), trans-pigment coherent time (6), ground state FMO energy gap (7), average binding affinities (8), average H-bonds (in ceiling function) (9) and average van der Waals (in ceiling function) (10)

of photophysical and quantum descriptors across all pigments in the gas phase (Fig. 5(a)) and solvent (SMD, water) (Fig. 5(b)). In both conditions, over 73% of the total variance is captured, confirming that the dimensionality reduction captures the majority of trait differences. In the gas phase (Fig. 5(a)), chlorophyll f and bacteriochlorophyll d stand apart due to their low energy barriers and long coherent times (variables 5 and 6). In contrast, chlorophyll c and bacteriochlorophyll e are separated by their low extinction coefficients and oscillator strengths (variables 3 and 4). Chlorophyll a, bacteriochlorophylls a, and g cluster near the center with balanced values, aligning with their robust and efficient roles in native systems. In the solvent condition (Fig. 5(b)), we observe a tighter clustering of several pigments (notably chlorophylls a and b, and bacteriochlorophylls a, b, g), indicating that the water solvent stabilizes specific properties, particularly enhancing extinction coefficient (4) and oscillator strength (3). Interestingly, chlorophyll f, bacteriochlorophyll d, and chlorophyll c remain outliers, underscoring their unique adaptation to niche light environments and distinct quantum characteristics even after solvation.

The eigenvector directions are distinctive between no solvent (Fig. 5(a)) and with solvent (Fig. 5(b)). Under no solvent condition, the eigenvectors show that excitation and absorption properties (i.e., energy gap, wavelength, oscillator strength, and extinction coefficient) align strongly along  $PC_1$ , while quantum transport traits (i.e., tunneling rate and coherence time) distribute more across  $PC_2$ . On the other hand, under solvent conditions, the influence of binding-related descriptors (i.e., H-bonds and van der Waals contacts) becomes more prominent on  $PC_2$ . At the same time, absorption properties remain dominant along  $PC_1$ . The results showed that most pigments cluster more tightly in the solvent, while chlorophylls c, f, and bacteriochlorophyll d remain distinct due to unique quantum traits. Excitation-related properties dominate  $PC_1$ , while  $PC_2$  reflects quantum or binding effects depending on the environment.

# The Pigments' Quantum Profile as a Complex System with Binding Protein

The calculations in this study reveal that all pigments possess distinct band gaps. Band gaps, or FMO energy gaps, indicate the kinetic interaction stability of pigments [40]. *In silico* docking studies suggest larger band gaps allow more stable interactions with protein receptors [41-42]. The docking results showed that chlorophyll c and bacteriochlorophylls c and d exhibit the strongest binding affinities, with no statistically significant differences between these three pigments (Fig. 5). Combining all the data, aside from the primary pigments, bacteriochlorophyll g emerges as a potential

candidate for substitution, as it exhibits a high extinction coefficient, tunneling rate, and coherent time. Further structural comparisons are needed to synthesize novel derivative pigments for improved photosynthesis and the engineering of photosynthetic systems.

computational Future studies should test chlorophyll and bacteriochlorophyll pigments components of multiple-pigment systems rather than single-pigment studies. For example, in the Photosystem II complex (RCSB ID: 5MDX), 212 chlorophyll a and 96 chlorophyll b molecules are involved, with 10-15 pigments housed in each chlorophyll-binding protein. Similarly, the Fenna-Matthews-Olson complex in bacteria like Chlorobium tepidum (RCSB ID: 3BSD) and Prosthecochloris aestuarii (RCSB: 6MEZ) hosts 7 bacteriochlorophylls per binding protein. Simulating pigments within a planar crystal system (e.g.,  $2 \times 2 \times 2$ matrices) using high-performance computational tools like Quantum Espresso (QE) [43] would better represent their electronic profiles within these biological systems.

# **Prospects in Synthetic Photosynthetic Biology**

This study aims to provide pigment characterization using DFT at the ground state and time-dependent simulation for photosynthetic characterization that can be used for future studies requiring deeper quantum mechanics characterization or supporting synthetic biology projects focused on engineering photosynthetic systems in cell-free environments or living organisms. One prospect involves engineering the pigment molecules (e.g., chlorophyll), redesigning light-harvesting complexes, introducing non-native pigments, or even combining them with de novo synthetic carbon fixation pathways and artificial reaction center development [44-46]. These ideas will be necessary for designing operational systems adapted to harsh or extreme environments, e.g., regions with high or low light intensity on Earth or even extraterrestrial environments like Mars or Venus, where sunlight may be dimmer or brighter.

However, several challenges must be overcomed, including tackling the complexities of photosynthetic systems, ensuring system stability, optimizing energy efficiency for total metabolism, and addressing genetic engineering limitations. These challenges can be mitigated

through state-of-the-art developments in modular design techniques, advanced modeling and simulation, directed evolution, and synthetic minimal organisms as testing "chassis". Additionally, system modeling combined with computational biology (such as DFT) can facilitate pigment characterization, guiding the selection of suitable pigments or aiding synthetic pigment design.

### CONCLUSION

This study characterized the pigment profiles of the chlorophylls and bacteriochlorophylls. The ground state DFT results favored chlorophylls a, b, and c as they highest exhibited the energy gaps. bacteriochlorophylls, g and b showed the highest energy gaps compared to the other pigments. In terms of exciton profiles, time-dependent DFT revealed that certain pigments respond to shorter wavelength spectrums (e.g., around 400 nm for chlorophylls a and b and bacteriochlorophylls a, b, and g), indicating their responsiveness to higher-energy photons. Conversely, chlorophyll other pigments (e.g., bacteriochlorophylls c, d, and e) respond to longer wavelengths (> 700 nm), enabling adaptation to lowlight conditions. The pigments could interact with the plant photosystem II chlorophyll-binding protein, but chlorophyll c and bacteriochlorophylls c and d demonstrated strongest binding the affinities. Additional calculations of quantum metrics (i.e., extinction coefficient, tunneling rate, and coherent time) indicated that bacteriochlorophyll g is a strong candidate for synthetic substitution. PCA results suggest that the pigments grouped into three clusters based on tunneling rate performance, while other properties were relatively similar. This study proposes that chlorophyll a and bacteriochlorophyll g are optimal for bright-light synthetic systems. In contrast, chlorophyll f and bacteriochlorophyll d may be better suited for dim or filtered-light environments. This work lays a foundation further computational and experimental development of engineered photosynthetic systems.

### ACKNOWLEDGMENTS

We are thankful to Mikhael Abidan Abednego (Physics Department, Universitas Indonesia) for his

guidance during the computational analysis.

### CONFLICT OF INTEREST

The authors have no conflict of interest to declare.

## AUTHOR CONTRIBUTIONS

Adhityo Wicaksono conceptualized the idea, helped with data collection, and supervised, including the methodology and software. Muhammad Ja'far Prakoso also helped with conceptualization and data collection and worked with the computation. Afif Maulana Yusuf Ridarto helped with conceptualization and chemistry analysis. Arli Aditya Parikesit supervised and validated the methodology. All authors contributed equally to the manuscript writing and finalization.

### **■ REFERENCES**

- [1] Baroch, M., and Dian, J., 2024, Electrochemical behavior of chlorophylls, bacteriochlorophylls, and related macrostructures—A review, *Monatsh. Chem.*, 155 (8), 771–782.
- [2] Buscemi, G., Vona, D., Trotta, M., Milano, F., and Farinola, G.M., 2022, Chlorophylls as molecular semiconductors: Introduction and state of art, *Adv. Mater. Technol.*, 7 (2), 2100245.
- [3] Shevela, D., Kern, J.F., Govindjee, G., and Messinger, J., 2023, Solar energy conversion by photosystem II: Principles and structures, *Photosynth. Res.*, 156 (3), 279–307.
- [4] Myśliwa-Kurdziel, B., Latowski, D., Strzałka, K., 2019, "Chlorophylls c—Occurrence, synthesis, properties, photosynthetic and evolutionary significance" in *Advances in Botanical Research*, vol. 90, Eds. Grimm, B., Academic Press, Cambridge, MA, US, 91–119.
- [5] Tsuzuki, Y., Tsukatani, Y., Yamakawa, H., Itoh, S., Fujita, Y., and Yamamoto, H., 2022, effects of light and oxygen on chlorophyll d biosynthesis in a marine cyanobacterium *Acaryochloris marina*, *Plants*, 11 (7), 915.
- [6] Mendili, M., and Khadhri, A., 2025, "Chlorophylls: The Verdant World of Photosynthetic Pigments" in Microbial Colorants: Chemistry, Biosynthesis and Applications, Eds. Rather, L.J., Shahid, M., and Jameel, S., Scrivener Publishing, Beverly, MA, US, 223–239.

- [7] Allakhverdiev, S.I., Kreslavski, V.D., Zharmukhamedov, S.K., Voloshin, R.A., Korol'kova, D.V., Tomo, T., and Shen, J.R., 2016, Chlorophylls d and f and their role in primary photosynthetic processes of cyanobacteria, *Biochemistry (Moscow)*, 81 (3), 201–212.
- [8] Chen, M., 2019, "Chlorophylls d and f: Synthesis, occurrence, light-harvesting, and pigment organization in chlorophyll-binding protein complexes" in *Advances in Botanical Research*, vol. 90, Eds. Grimm, B., Academic Press, Cambridge, MA, US, 121–139.
- [9] Pareek, S., Sagar, N.A., Sharma, S., Kumar, V., Agarwal, T., González-Aguilar, G.A., and Yahia, E.M., 2017, "Chlorophylls: Chemistry and biological functions" in *Fruit and Vegetable Phytochemicals: Chemistry and Human Health*, 2<sup>nd</sup> Ed., Wiley-Blackwell, Hoboken, NJ, US, 269–284.
- [10] Guberman-Pfeffer, M.J., 2019, Mechanisms of Porphyrinoid and Carotenoid Spectral Tuning Revealed with Quantum Chemistry, *Dissertations*, University of Connecticut, US.
- [11] Govindjee, G., Stirbet, A., Lindsey, J.S., and Scheer, H., 2024, On the Pelletier and Caventou (1817, 1818) papers on chlorophyll and beyond, *Photosynth. Res.*, 160 (1), 55–60.
- [12] da Silva, J.C., and Lombardi, A.T., 2020. "Chlorophylls in Microalgae: Occurrence, Distribution, and Biosynthesis" in *Pigments from Microalgae Handbook*, Eds. Jacob-Lopes, E., Queiroz, M., and Zepka, L., Springer International Publishing, Cham, Switzerland, 1–18.
- [13] Wang, P., and Grimm, B., 2015, Organization of chlorophyll biosynthesis and insertion of chlorophyll into the chlorophyll-binding proteins in chloroplasts, *Photosynth. Res.*, 126 (2), 189–202.
- [14] Tanaka, K., and Chujo, Y., 2021, New idea for narrowing an energy gap by selective perturbation of one frontier molecular orbital, *Chem. Lett.*, 50 (2), 269–279.
- [15] Zhu, Z., Higashi, M., and Saito, S., 2022, Excited states of chlorophyll a and b in solution by time-dependent density functional theory, *J. Chem. Phys.*,

- 156 (12), 124111.
- [16] Sokolov, M., and Cui, Q., 2025, Impact of fluctuations in the peridinin-chlorophyll a-protein on the energy transfer: Insights from classical and QM/MM molecular dynamics simulations, *Biochemistry*, 64 (4), 879–894.
- [17] Saito, K., Suzuki, T., and Ishikita, H., 2018, Absorption-energy calculations of chlorophyll a and b with an explicit solvent model, *J. Photochem. Photobiol.*, *A*, 358, 422–431.
- [18] Poddubnyy, V.V., Kozlov, M.I., and Glebov, I.O., 2021, The origin of the red shift of Q<sub>y</sub> band of chlorophylls d and f, *Chem. Phys. Lett.*, 778, 138792.
- [19] Takabayashi, Y., Sato, H., and Higashi, M., 2023, Theoretical analysis of the coordination-state dependency of the excited-state properties and ultrafast relaxation dynamics of bacteriochlorophyll a, *Chem. Phys. Lett.*, 826, 140669.
- [20] Frisch, M.J., Trucks, G.W., Schlegel, H.B., Scuseria, G.E., Robb, M.A., Cheeseman, J.R., Scalmani, G., Barone, V., Mennucci, B., Petersson, G.A., Nakatsuji, H., Caricato, M., Li, X., Hratchian, H.P., Izmaylov, A.F., Bloino, J., Zheng, G., Sonnenberg, J.L., Hada, M., Ehara, M., Toyota, K., Fukuda, R., Hasegawa, J., Ishida, M., Nakajima, T., Honda, Y., Kitao, O., Nakai, H., Vreven, T., Montgomery, J.A., Jr., Peralta, J.E., Ogliaro, F., Bearpark, M., Heyd, J.J., Brothers, E., Kudin, K.N., Staroverov, V.N., Kobayashi, R., Normand, J., Raghavachari, K., Rendell, A., Burant, J.C., Iyengar, S.S., Tomasi, J., Cossi, M., Rega, N., Millam, J.M., Klene, M., Knox, J.E., Cross, J.B., Bakken, V., Adamo, C., Jaramillo, J., Gomperts, R., Stratmann, R.E., Yazyev, O., Austin, A.J., Cammi, R., Pomelli, C., Ochterski, J.W., Martin, R.L., Morokuma, K., Zakrzewski, V.G., Voth, G.A., Salvador, P., Dannenberg, J.J., Dapprich, S., Daniels, A.D., Farkas, Ö., Foresman, J.B., Ortiz, J.V., Cioslowski, J., and Fox, D.J., 2013, Gaussian-09 Revision D.01, Gaussian, Inc., Wallingford, CT.
- [21] O'Boyle, N.M., Banck, M., James, C.A., Morley, C., Vandermeersch, T., and Hutchison, G.R., 2011, Open Babel: An open chemical toolbox, *J. Cheminf.*, 3 (1), 33.

- [22] Trott, O., and Olson, A.J., 2010, AutoDock Vina: Improving the speed and accuracy of docking with a new scoring function, efficient optimization, and multithreading, *J. Comput. Chem.*, 31 (2), 455–461.
- [23] Schrödinger, LLC, 2015, *The PyMOL Molecular Graphics System*, Version 3.1.3.
- [24] Tatsumi, Y., and Saito, R., 2018, Interplay of valley selection and helicity exchange of light in Raman scattering for graphene and MoS<sub>2</sub>, *Phys. Rev. B*, 97 (11), 115407.
- [25] Becke, A.D., 1988, Density-functional exchangeenergy approximation with correct asymptotic behavior, *Phys Rev A*, 38 (6), 3098–3100.
- [26] Lee, C., Yang, W., and Parr, R.G., 1988, Development of the Colle-Salvetti correlation-energy formula into a functional of the electron density, *Phys. Rev. B*, 37 (2), 785–789.
- [27] Yanai, T., Tew, D.P., and Handy, N.C., 2004, A new hybrid exchange–correlation functional using the Coulomb-attenuating method (CAM-B3LYP), *Chem. Phys. Lett.*, 393 (1), 51–57.
- [28] Marenich, A.V., Cramer, C.J., and Truhlar, D.G., 2009, Performance of SM6, SM8, and SMD on the SAMPL1 test set for the prediction of small-molecule solvation free energies, *J. Phys. Chem. B*, 113 (14), 4538–4543.
- [29] Yan, J., Rodríguez-Martínez, X., Pearce, D., Douglas, H., Bili, D., Azzouzi, M., Eisner, F., Virbule, A., Rezasoltani, E., Belova, V., Dörling, B., Few, S., Szumska, A.A., Hou, X., Zhang, G., Yip, H.L., Campoy-Quiles, M., and Nelson, J., 2022, Identifying structure–absorption relationships and predicting absorption strength of non-fullerene acceptors for organic photovoltaics, *Energy Environ. Sci.*, 15 (7), 2958–2973.
- [30] Zeng, L., Wang, Y., and Zhou, J., 2016, Spectral analysis on origination of the bands at 437 nm and 475.5 nm of chlorophyll fluorescence excitation spectrum in *Arabidopsis* chloroplasts, *Luminescence*, 31 (3), 769–774.
- [31] Kume, A., Akitsu, T., and Nasahara, K.N., 2018, Why is chlorophyll b only used in light-harvesting systems?, *J. Plant Res.*, 131 (6), 961–972.

- [32] Heidenreich, K.M., and Richardson, T.L., 2020, Photopigment, absorption, and growth responses of marine cryptophytes to varying spectral irradiance, *J. Phycol.*, 56 (2), 507–520.
- [33] Hintz, N.H., Zeising, M., and Striebel, M., 2021, Changes in spectral quality of underwater light alter phytoplankton community composition, *Limnol. Oceanogr.*, 66 (9), 3327–3337.
- [34] Kaucikas, M., Nürnberg, D., Dorlhiac, G., Rutherford, A.W., and van Thor, J.J., 2017, Femtosecond visible transient absorption spectroscopy of chlorophyll f-containing photosystem I, *Biophys. J.*, 112 (2), 234–249.
- [35] Emeliantsev, P.S., Zhiltsova, A.A., Krasnova, E.D., Voronov, D.A., Rymar, V.V., and Patsaeva, S.V., 2020, Quantification of chlorosomal bacteriochlorophylls using absorption spectra of green sulfur bacteria in natural water, *Moscow Univ. Phys. Bull.*, 75 (2), 137–142.
- [36] Borah, K.D., and Bhuyan, J., 2017, Magnesium porphyrins with relevance to chlorophylls, *Dalton Trans.*, 46 (20), 6497–6509.
- [37] Simkin, A.J., Kapoor, L., Doss, C.G.P., Hofmann, T.A., Lawson, T., and Ramamoorthy, S., 2022, The role of photosynthesis related pigments in light harvesting, photoprotection and enhancement of photosynthetic yield in planta, *Photosynth. Res.*, 152 (1), 23–42.
- [38] Vaz, B., and Pérez-Lorenzo, M., 2023, Unraveling structure–performance relationships in porphyrinsensitized TiO<sub>2</sub> photocatalysts, *Nanomaterials*, 13 (6), 1097.
- [39] Tros, M., Mascoli, V., Shen, G., Ho, M.Y., Bersanini, L., Gisriel, C.J., Bryant, D.A., and Croce, R., 2021, Breaking the red limit: Efficient trapping of long-wavelength excitations in chlorophyll-f-containing photosystem I, *Chem*, 7 (1), 155–173.
- [40] Shahab, S., Sheikhi, M., Filippovich, L., Khaleghian,

- M., Dikusar, E., Yahyaei, H., and Borzehandani, M.Y., 2018, Spectroscopic studies (geometry optimization, E→Z isomerization, UV/Vis, excited states, FT-IR, HOMO-LUMO, FMO, MEP, NBO, polarization) and anisotropy of thermal and electrical conductivity of new azomethine dyes in stretched polymer matrix, *Silicon*, 10 (5), 2361–2385.
- [41] Mumit, M.A., Pal, T.K., Alam, M.A., Islam, M.A.A.A.A., Paul, S., and Sheikh, M.C., 2020, DFT studies on vibrational and electronic spectra, HOMO–LUMO, MEP, HOMA, NBO and molecular docking analysis of benzyl-3-*N*-(2,4,5-trimethoxyphenylmethylene)hydrazinecarbodithio ate, *J. Mol. Struct.*, 1220, 128715.
- [42] Janani, S., Rajagopal, H., Muthu, S., Aayisha, S., and Raja, M., 2021, Molecular structure, spectroscopic (FT-IR, FT-Raman, NMR), HOMO-LUMO, chemical reactivity, AIM, ELF, LOL and molecular docking studies on 1-benzyl-4-(*N*-Bocamino)piperidine, *J. Mol. Struct.*, 1230, 129657.
- [43] Giannozzi, P., Baseggio, O., Bonfà, P., Brunato, D., Car, R., Carnimeo, I., Cavazzoni, C., de Gironcoli, S., Delugas, P., Ferrari Ruffino, F., Ferretti, A., Marzari, N., Timrov, I., Urru, A., and Baroni, S., 2020, Quantum ESPRESSO toward the exascale, *J. Chem. Phys.*, 152 (15), 154105.
- [44] Erb, T.J., 2024, Photosynthesis 2.0: Realizing new-to-nature CO<sub>2</sub>-fixation to overcome the limits of natural metabolism, *Cold Spring Harbor Perspect. Biol.*,16 (2), a041669.
- [45] Batista-Silva, W., da Fonseca-Pereira, P., Martins, A.O., Zsögön, A., Nunes-Nesi, A., and Araújo, W.L., 2020, Engineering improved photosynthesis in the era of synthetic biology, *Plant Commun.*, 1 (2), 100032.
- [46] Leister, D., 2019, Genetic engineering, synthetic biology and the light reactions of photosynthesis, *Plant Physiol.*, 179 (3), 778–793.